Difluoromethyl-1,3,4-oxadiazoles are selective, mechanism-based, and essentially irreversible inhibitors of histone deacetylase 6

Beate König,[a,b] Paris R. Watson,[b] Nina Reßing,[a] Abigail D. Cragin,[b] Linda Schäker-Hübner,[a] David W. Christianson[*b] and Finn K. Hansen[*a]

[a]*Department of Pharmaceutical and Cell Biological Chemistry, Pharmaceutical Institute, University of Bonn, An der Immenburg 4, 53121 Bonn, Germany.*

[b]*Roy and Diana Vagelos Laboratories, Department of Chemistry, University of Pennsylvania, 231 South 34th Street, Philadelphia, Pennsylvania 19104-6323, United States.*

Abstract

Histone deacetylase 6 (HDAC6) is an important drug target in oncology and non-oncological diseases. Most available HDAC6 inhibitors (HDAC6i) utilize a hydroxamic acid as zinc-binding group which limits the therapeutic opportunities due its genotoxic potential. Recently, difluoromethyl-1,3,4-oxadiazoles (DFMOs) were reported as potent and selective HDAC6i, but their mode of inhibition remained enigmatic. Herein, we report that DFMOs act as mechanism-based and essentially irreversible HDAC6i. Biochemical data confirm that DFMO **6** is a tight-binding HDAC6i capable of inhibiting HDAC6 via a two-step slow-binding mechanism. Crystallographic and mechanistic experiments suggest that the attack of **6** by the zinc-bound water at the sp^2 carbon closest to the difluoromethyl moiety followed by a subsequent ring opening of the oxadiazole yields the deprotonated difluoroacetylhydrazide **13** as active species. The strong anionic zinc coordination of **13** and the binding of the difluoromethyl moiety in the P571 pocket finally results in an essentially irreversible inhibition of HDAC6.

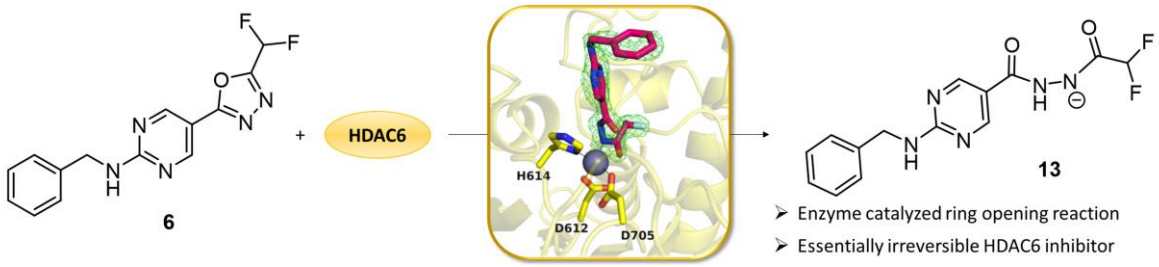

Introduction

Histone deacetylases (HDACs) are epigenetic drug targets that have originally been assumed to modify histone modifications by removing acetyl groups from lysine residues. Meanwhile, however, it has turned out that the substrate spectrum of the enzyme family is more complex.[1] In agreement with the usual division into four classes, it is now clear that only class I HDACs (HDACs 1, 2, 3, and 8) actually regulate histones.[1] Class III HDACs differ from the other zinc-dependent isoforms by the fact that they are NAD^+-dependent, whereas class IV consists of no more than one isoform, HDAC11, whose biological role is yet unclear.[2,3] A more versatile class of HDACs is class II with class IIa enzymes (HDACs 4, 5, 7, 9) playing a crucial role in gene expression, despite their poor deacetylase qualities.[1,4–6] Class IIb, on the other hand, includes HDAC6 and the polyamine deacetylase HDAC10 which are both mainly located in the cytosol.[1,7,8] Tailored to fit the highly-conserved active sites of the different isoforms, HDAC inhibitors (HDACi) typically consist of a zinc-binding group (ZBG), a variably sized cap group and a suitable linker connecting the two units.[9] In contrast to unselective or class I-specific HDAC inhibition by HDACi such as vorinostat, belinostat, panobinostat, and romidepsin, which have been introduced as FDA-approved anticancer drugs in the past two decades, HDAC6 inhibition has no effect on histones and is thus presumed to cause less severe adverse effects.[10,11] Originally considered to be a tubulin deacetylase, HDAC6 has since been found to regulate a range of other proteins as well; most notably cortactin, the Alzheimer-related tau, and the chaperone Hsp90.[7,12–15] Serving this particular range of substrates, HDAC6 regulation has been investigated as a promising treatment option for non-oncological conditions, for example neurodegenerative diseases[13,14,16,17], several rare disorders, like Rett syndrome and Charcot-Marie-Tooth disease[18,19], autoimmune diseases, and other chronic conditions including idiopathic pulmonary fibrosis and inflammasome-mediated disorders.[20–22] Through enabling aggresome formation, HDAC6 is further involved in cellular protein degradation which makes it a prominent target for synergistic drug combination approaches with proteasome inhibitors.[23–25] On the clinical level, this synergism is already being addressed by the combination of bortezomib, dexamethasone, and the pan-HDACi panobinostat for the treatment of multiple myeloma while further combination studies using the HDAC6-preferential inhibitor ricolinostat are ongoing.[26]

Other promising targets for synergistic activities with HDAC6i that are currently being investigated include BET-proteins[27,28], topoisomerases[29], the lysine-specific demethylase 1 (LSD1)[30–33], and Hsp90[34–38]. In consequence, and despite having limited clinical anticancer potential on its own, HDAC6 has turned out as a prominent drug target for combination therapies but only few of the many selective HDAC6i presented so far have yet entered clinical trials.[39–42] One major limitation in this regard seems to be the fact that most HDAC6i incorporate hydroxamate ZBGs which affect the drug's tolerability and overall performance by promoting off-target interactions and the appearance of toxic metabolites. In fact, hydroxamate groups have long been suspected of releasing hydroxylamine or undergoing the Lossen rearrangement yielding isocyanates under physiological conditions.[11,43] Given that both species are highly mutagenic and thus unsuitable for long-term therapy, there is an urgent need for alternative ZBGs but even after several years of intensive research, there are only few candidates with pleasing chelating properties and low toxicity levels.[44] Beside ethyl hydrazides[45] and several non-hydroxamate compounds of yet undisclosed structures that are currently in phase II trials, the most promising HDAC6-selective binding motif seems to be the difluoromethyl-1,3,4-oxadiazole (DFMO) group that has been discovered by Kim *et al*.[46] According to their study, the DFMO group exhibited excellent HDAC6 inhibition in the low nanomolar concentration range with a high selectivity over HDAC1.[46] Furthermore, the DFMO group was successfully utilized in HDAC6 selective inhibitors to overcome leptin resistance in obesity and in HDAC6-selective proteolysis-targeting chimeras (PROTACs).[47,48]

In 2022, we reported on a DFMO derivative that underwent a ring opening reaction in the presence of HDAC6 leading to a acylhydrazide which was successfully co-crystallized in an extended conformation in the active site of HDAC6.[49] Shortly after our initial disclosure Steinkühler and co-workers observed a similar ring opening reaction followed by a hydrolysis reaction yielding a hydrazide derivative which was crystallized in complex with HDAC6.[50] Herein, we report the full experimental details of our initial conference abstract demonstrating that difluoromethyl-1,3,4-oxadiazoles act as selective, mechanism-based, and essentially irreversible inactivators capable of inhibiting HDAC6 via a two-step slow-binding mechanism.

Results and Discussion

Design, synthesis, and HDAC inhibition of difluoromethyloxadiazole-based HDAC6 inhibitors

To identify key structural requirements for selective HDAC6 inhibition by DFMO-derived inhibitors, we decided to pursue a fragment-based approach. In the first step, to investigate the influence of the (hetero)aromatic linker, HDAC6i fragments containing phenyl (**1**), pyridinyl (**2**), and pyrimidinyl (**3**) linkers attached to the DFMO ZBG were included in the design and synthesis of initial prototypic compounds. For the synthesis of the fragments **1**, **2**, and **3** the respective carbonitriles were transformed into the corresponding tetrazoles by the treatment with sodium azide, followed by the reaction with difluoroacetic anhydride (DFAA) to generate the DFMO group *via* a Huisgen 1,3,4-oxadiazole synthesis (see Scheme S1, Supporting Information).[51] The three synthesized fragments were screened for their inhibition of HDAC6 and HDAC1-4 using biochemical HDAC inhibition assays. The pyrimidinyl derivative **3** displayed the highest inhibitory potency against HDAC6, while all fragments were inactive against the control isoforms HDAC1-4 (Table 1).

Due to the initial activity of the pyrimidinyl fragment **3**, we designed full sized HDACi including a benzyl as well as a *para*-methoxy benzyl cap group, an aminopyrimidinyl linker, and the DFMO ZBG. To obtain **6** and **7** the respective benzylamines were subjected to a nucleophilic aromatic substitution reaction with 2-chloropyrimidine-5-carbonitrile. The resulting carbonitrile intermediates were converted into the corresponding DFMO derivatives as described above (Scheme 1A). In subsequent HDAC inhibition assays we observed submicromolar inhibitory activities against HDAC6 for both full-sized HDAC6i (**6** and **7**), with IC_{50} values of 0.193 µM and 0.337 µM, respectively, and no activity against HDAC1-4 (Table 1).

Additionally, the DFMO ZBG was introduced in potent well-established HDAC6i such as nexturastat A and our previously published peptoid-based HDAC6i.[52,53] For the synthesis of the nexturastat derivatives (**9**, **10**), *n*-butylamine was alkylated with methyl 4-(bromomethyl)benzoate. Next, the resulting intermediate **8** was treated with phenyl phenylcarbamate or benzoyl chloride to provide the corresponding urea and carboxamide derivatives. The respective products were subjected to a hydrazinolysis followed by a difluoroacetylation reaction with DFAA. The resulting acylhydrazides were converted into

the desired DFMO ZBG *via* a dehydrative cyclization reaction using Burgess reagent (Scheme 1B). The peptoid derivative (**12**) was synthesized starting from an Ugi four-component reaction.[53,54] The formation of the DFMO moiety was accomplished in three steps from methyl ester intermediate **11** *via* the hydrazinolysis, difluoroacetylation, and dehydrative cyclization sequence described above (Scheme 1C). Interestingly, the nexturastat A analogs **9** and **10** and the peptoid-based HDACi **12** displayed only moderate inhibitory activity against HDAC6 and were inactive against HDAC1-4. The typical structural features of selective hydroxamate-based HDAC6i include a benzyl linker in combination with a bulky or branched cap group.[55] Our results for the DFMO derivatives **9**, **10**, and **12** indicate that this HDAC6 pharmacophore cannot be directly translated to DFMO-based HDAC6i. A possible explanation for this phenomenon could be a different binding mode in the active site of HDAC6. Due to the highest HDAC6 inhibitory activity in this set of compounds, we selected **6** for elucidating its binding mode in the second catalytic domain 2 (CD2) of *Danio rerio* (zebrafish) HDAC6.

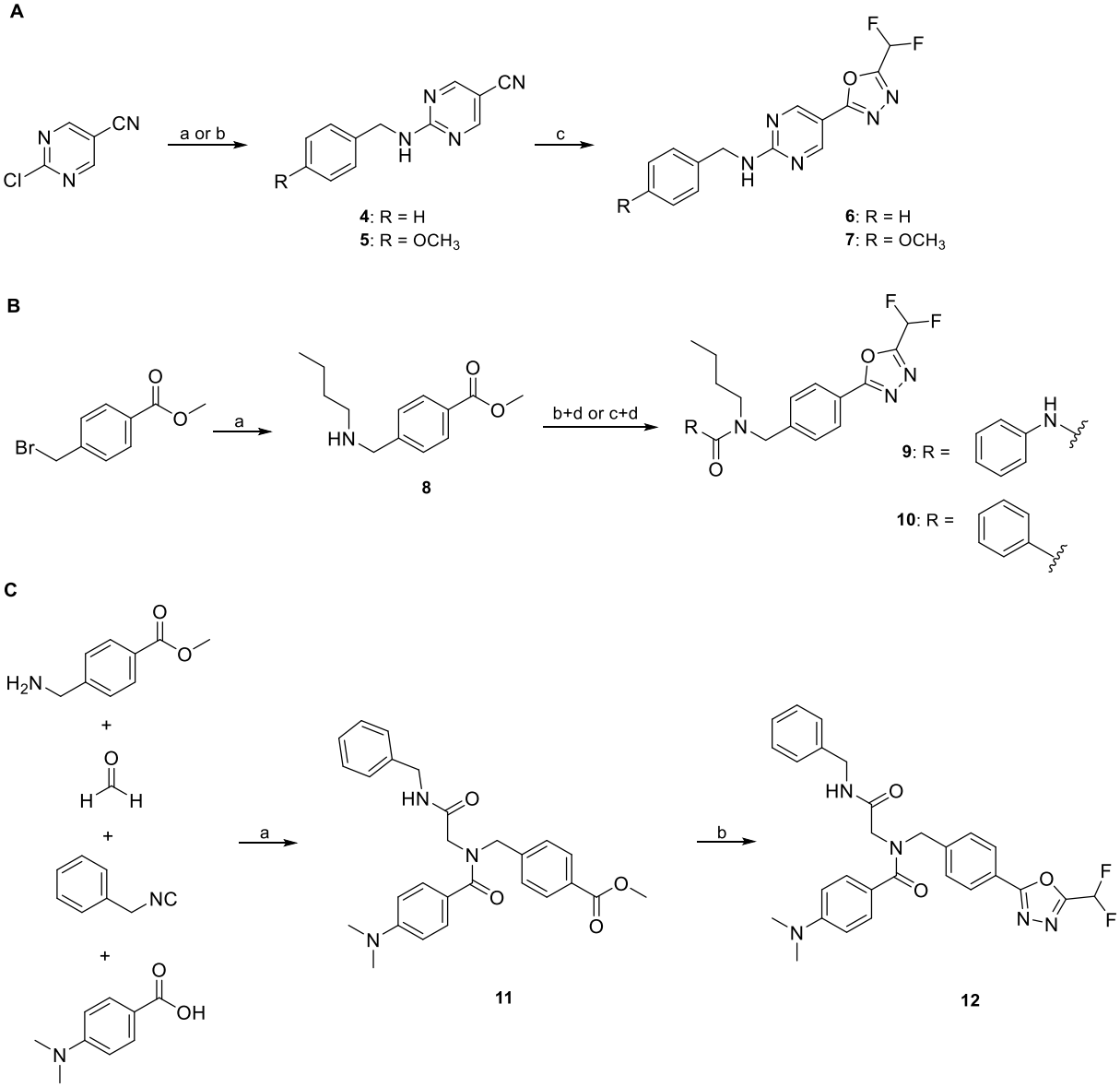

Scheme 1. A: Synthesis of full sized HDAC6i **6** and **7**. a) Benzylamine, DIPEA, EtOH, 90 °C, 18 h (**4**); b) 4-methoxybenzylamine, DIPEA, EtOH, 90 °C, 18 h (**5**); c) i: NaN_3, NH_4Cl, $LiCl{\cdot}H_2O$, DMF, 100 °C, 18 h; ii: DFAA. **B:** Synthesis of nexturastat analogs **9** and **10**. a) *n*-Butylamine, THF, rt., 3 h; b) phenyl phenylcarbamate, TEA, THF, 66 °C, 2 h (**9**); c) benzoyl chloride, CH_2Cl_2, rt., 2 h (**10**); d) i: hydrazine monohydrate, MeOH, 70 °C, 3 h; ii: DFAA, DMF, 70 °C, 1 h; iii: burgess reagent, THF, 60 °C, 18 h. **C:** Synthesis of the peptoid-based HDACi **12**. a) TEA, MeOH, rt., 72 h; b) i: hydrazine monohydrate, MeOH, 70 °C, 3 h; ii: DFAA, TEA, DMF, 70 °C, 1 h; iii: burgess reagent, TEA, THF, 60 °C, 18 h.

Table 1. Inhibitory activities of the synthesized difluoromethyl-1,3,4-oxadiazoles against HDAC6 and the control isoforms HDAC1-4; IC_{50} values [µM, mean ± SD] or percent inhibition at 10 µM; n. e.: no effect = < 15% inhibition at 10 µM; n. d.: not determined.[a]

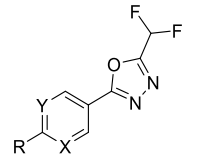

1: X = CH; Y = CH; R = H
2: X = N; Y = CH; R = CH_3
3: X = N; Y = N; R = H

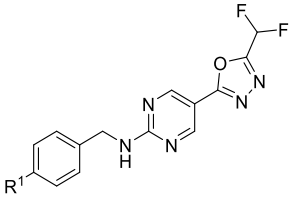

6: R = H
7: R = OCH_3

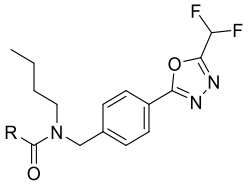

9: R= NH-phenyl
10: R= phenyl

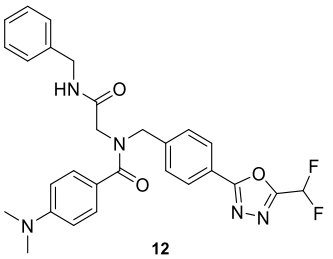

12

Cpd	HDAC6	HDAC1	HDAC2	HDAC3	HDAC4
1	n. e.	n. e.	n. e.	n. e.	n. e.
2	39%	n. e.	n. e.	n. e.	n. e.
3	56%	n. e.	n. e.	n. e.	n. e.
6	0.193 ± 0.006 µM	n. e.	n. e.	n. e.	n. e.
7	0.337 ± 0.026 µM	n. e.	n. e.	n. e.	n. e.
9	76%	n. e.	n. e.	n. e.	n. e.
10	75%	n. e.	n. e.	n. e.	n. e.
12	27%	n. e.	n. e.	n. e.	n. e.
Vorinostat	0.039 ± 0.005 µM	0.128 ± 0.009 µM	0.158 ± 0.033 µM	0.079 ± 0.016 µM	n. d.
TMP-269	n. d.	n. d.	n. d.	n. d.	0.753 ± 0.010 µM

[a]preincubation of HDAC1-4 or 6 and inhibitor: 1 h at 25 °C.

*Compound **6** is a substrate analog of HDAC6 that undergoes an enzyme-catalyzed ring opening reaction*

Oxadiazole **6** was cocrystallized with HDAC6, and crystals diffracted X-rays to 2.00 Å resolution. The initial electron density map of the enzyme-inhibitor complex was phased by molecular replacement using the structure of the unliganded enzyme (PDB 5EEM)[56] as a search probe for rotation and translation function calculations. After a molecular replacement solution was achieved and initial rounds of crystallographic structure refinement were completed, we attempted to fit oxadiazole **6** into strong $|F_o|-|F_c|$ difference electron density in the active site (Figure 1A, B). Surprisingly, the intact oxadiazole would not fit satisfactorily in this electron density map (Figure 1C). After studying the electron density map and considering the possible reactivity of the oxadiazole moiety, we concluded that the oxadiazole ring had undergone nucleophilic attack by the zinc-bound water to yield a ring-opened form – acylhydrazide **13** – which fits the initial, unbiased electron density map perfectly (Figure 1D). The structure of the HDAC6–**13** complex was refined to convergence with R/R_{free} = 0.185/0.223.

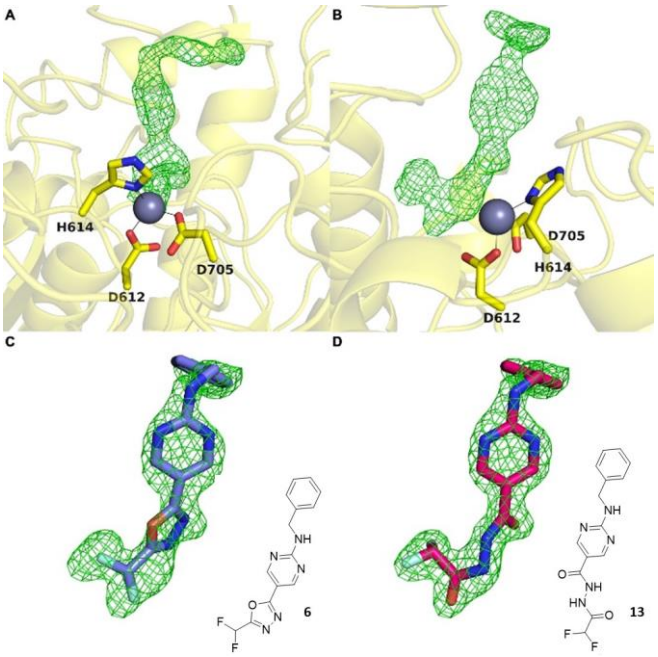

Figure 1. The initial $|F_o|-|F_c|$ map (two orientations (**A**) and (**B**)) calculated from X-ray diffraction data collected from crystals of HDAC6 cocrystallized with inhibitor **6** reveals strong, unbiased electron density for the bound inhibitor in the active site. Surprisingly, this difference density could not be fit satisfactorily with intact oxadiazole **6** (**C**); instead, it could

be fit perfectly with acylhydrazide **13** resulting from hydrolysis and ring-opening of the oxadiazole (**D**).

A Polder omit map of the final enzyme-inhibitor complex is shown in Figure 2A. Inhibitor binding does not trigger any major structural changes in the protein, and the root-mean-square deviation is 0.177 Å for 315 Cα atoms between the inhibitor-bound and unliganded enzyme (PDB 5EEM). Interestingly, the structure reveals an extensive array of intermolecular interactions that stabilize the bound inhibitor (Figure 2B). Key among these interactions is coordination of an acylhydrazide nitrogen to the catalytic zinc ion (N•••Zn^{2+} distance = 2.0 Å). This interaction requires deprotonation of the acylhydrazide NH group to form a nitrogen anion – this could result directly from the mechanism of ring-opening, or it could result from deprotonation of the neutral acylhydrazide (as discussed later).

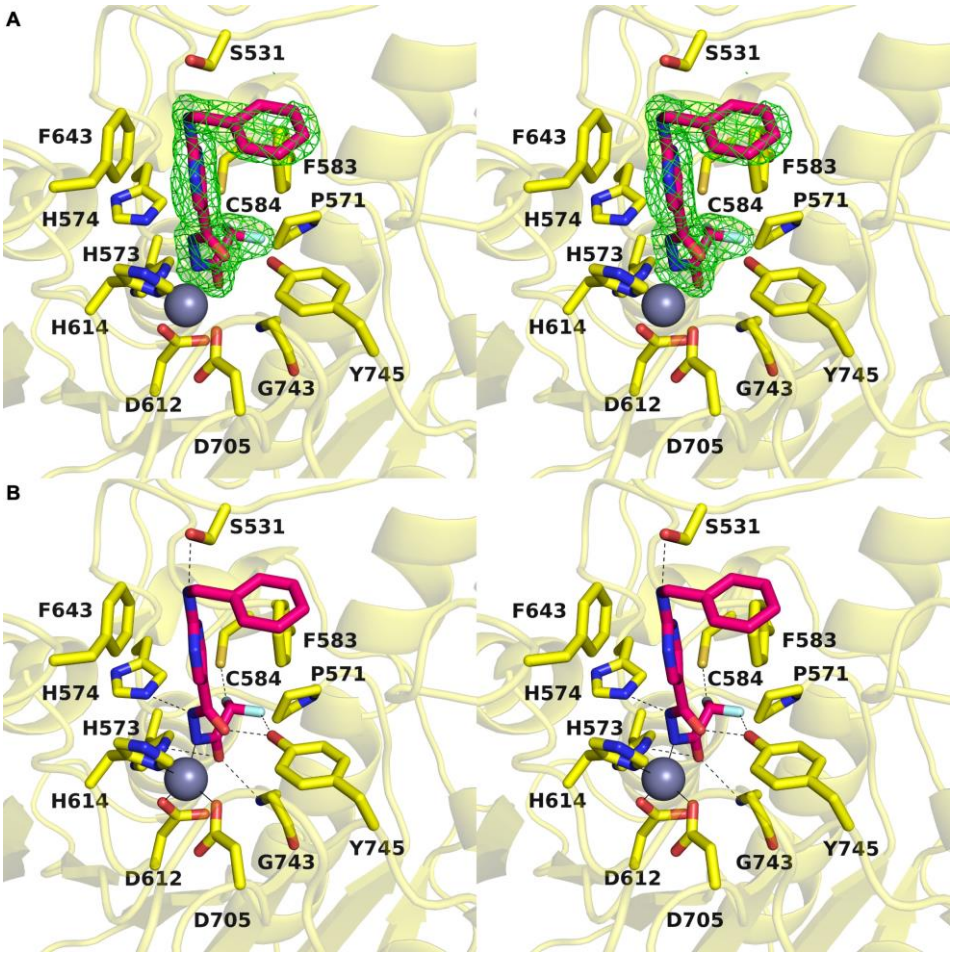

Figure 2. A: Stereoview of the Polder omit map of **13** contoured at 3σ. **B**: Stereoview highlighting intermolecular interactions in the enzyme-inhibitor complex in the active site of HDAC6. The catalytic zinc ion is shown as a gray sphere; metal coordination and hydrogen bond interactions are shown as solid and dashed black lines, respectively.

The bound inhibitor makes numerous hydrogen bond interactions with active site residues. One carbonyl group of the acylhydrazide forms hydrogen bonds with H574 and the backbone NH group of G743, and the other carbonyl group forms a hydrogen bond with Y745. Interestingly, both C–F groups engage in hydrogen bond interactions: one C–F group forms a hydrogen bond with C584 and the other forms a hydrogen bond with Y745. Finally, the benzylamino NH group forms a hydrogen bond with S531, and both aromatic rings of the inhibitor engage in offset stacked and edge-to-face aromatic interactions with F583 and F643.

Overlay of the structure of the HDAC6 complex with acylhydrazide **13** and the recently-reported structure of the HDAC6 complex with a hydrazide resulting from hydrolysis of another oxadiazole inhibitor (PDB 8A8Z)[50] reveals slight shifts of 0.9 Å in the orientation of the zinc-binding group and the aromatic linker region; unlike the situation for zinc coordination by an amide NH group, the primary amino group of the hydrazide does not have to be deprotonated to coordinate to zinc (Figure 3). Other differences between the binding of acylhydrazide and hydrazide inhibitors include the hydrogen bond with catalytic tyrosine Y745, which at 2.1 Å is 0.4 Å shorter in the complex with the hydrazide (making this a very short hydrogen bond), and the binding of a water molecule in the P571 pocket.

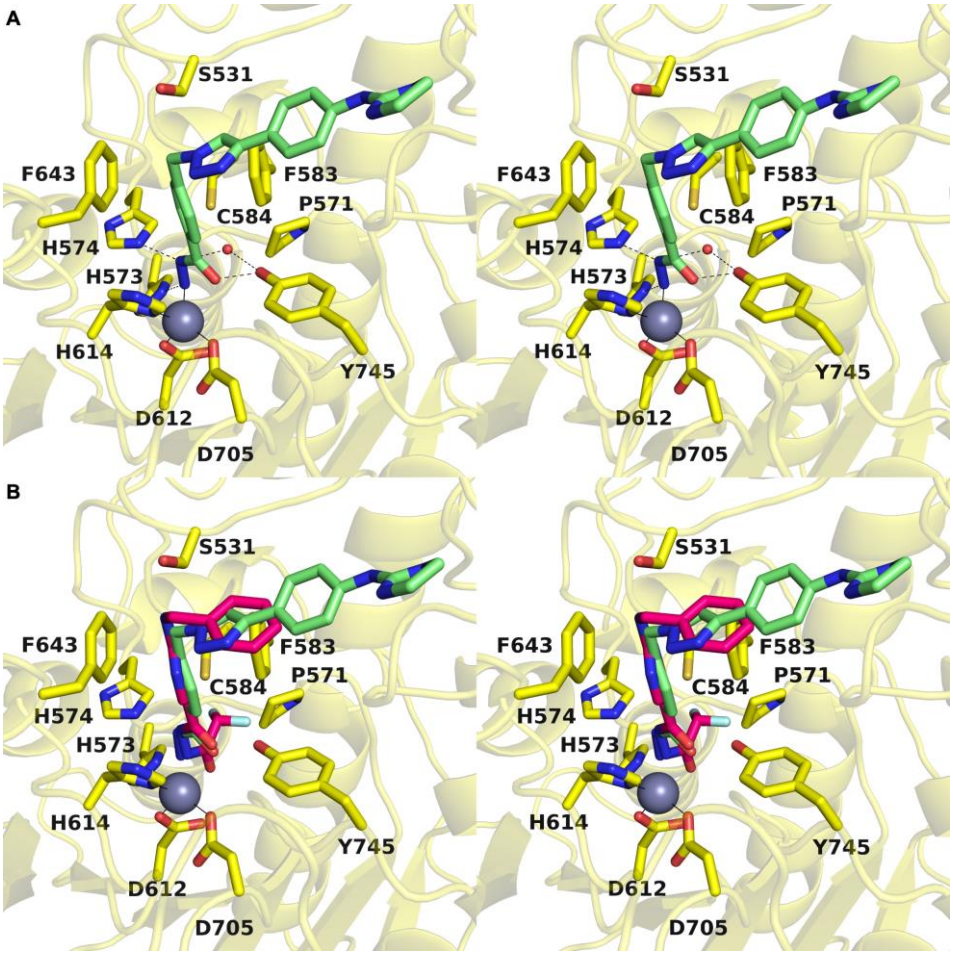

Figure 3. A: Stereoview of the oxadiazole-derived hydrazide inhibitor bound in the active site of HDAC6 (PDB 8A8Z). **B**: Overlay of the oxadiazole-derived acylhydrazide and hydrazide inhibitors bound in the active site of HDAC6.

Difluoromethyl-1,3,4-oxadiazoles are mechanism-based and essentially irreversible HDAC6 inhibitors

The enzyme-catalyzed ring opening reaction observed for **6** in the presence of HDAC6 prompted us to investigate the structural requirements for this unique mode of action in detail. To this end, we synthesized the cocrystallized acylhydrazide **13** as a reference compound as well as the corresponding trifluoromethyl-1,3,4-oxadiazole (**14**) and methyl-1,3,4-oxadiazole (**15**) analogs of **6** (Figure 4; see Scheme S3 for synthetic details, Supporting Information). The subsequent HDAC6 inhibition assays revealed that the acylhydrazide **13**

and the methyl-1,3,4-oxadiazole derivative **15** displayed only very weak inhibitory properties with less than 15% inhibition at the highest concentration tested (10 µM). In contrast, the trifluoromethyl-1,3,4-oxadiazole **14** displayed submicromolar HDAC6 inhibitory activity against HDAC6 (IC_{50}: 0.531 µM) and no inhibition of the four control isoforms HDAC1-4. Consequently, we focused on the difluoromethyl-1,3,4-oxadiazole **6** and the trifluoromethyl-1,3,4-oxadiazole **14** in our in-depth evaluation of the binding kinetics. Most hydroxamates are HDACi with fast-on and fast-off binding kinetics, while HDACi with alternative ZBGs such as aminoanilides and alkyl hydrazides are often slow- and tight-binding inhibitors.[57–59] To investigate whether **6** and **14** display slow-on binding properties we performed HDAC6 inhibition assays with different preincubation times using vorinostat as control; the results are summarized in Figure 5A. As expected, the HDAC6 inhibition by vorinostat did not depend on the preincubation time. In contrast, the observed concentration-effect curves of **6** and thus the IC_{50} values were highly dependent on the preincubation time (5 min IC_{50}: 0.347 µM; 1 h IC_{50}: 0.193 µM; 2 h IC_{50}: 0.129 µM), thereby indicating a slow-binding profile. Similarly, **14** also showed a substantial decrease in the HDAC6 IC_{50} values upon preincubation (5 min IC_{50}: 0.840 µM; 1 h IC_{50}: 0.531 µM; 2 h IC_{50}: 0.601 µM).

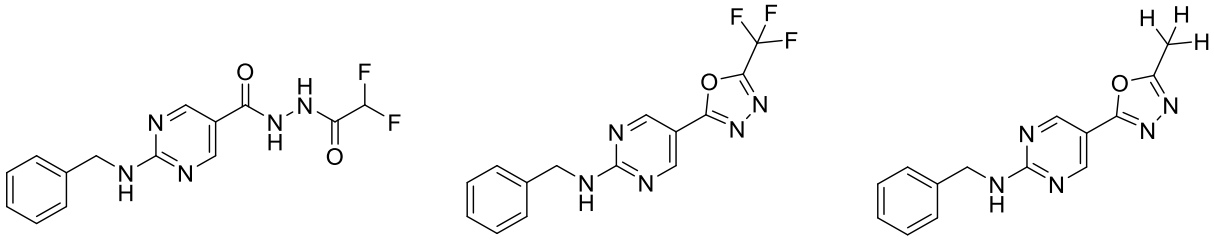

Figure 4. Structures of the acylhydrazide (**13**), trifluoromethyl-1,3,4-oxadiazole (**14**) and methyl-1,3,4-oxadiazole (**15**) analogs. Inhibitory activities of prepared compounds against HDAC1-4 and HDAC6; IC_{50} [µM, mean ± SD]; n.e.: no effect = < 15% inhibition at 10 µM.

To determine whether **6** and **14** are tight-binding inhibitors of HDAC6, we analyzed the dissociation behavior of both compounds by 100-fold jump dilution experiments using vorinostat as control. Briefly, HDAC6 in assay buffer was incubated with an excess of the respective inhibitor (at least 10-fold IC_{50}) or with blank (DMSO 1%) for 1 hour at room temperature. Subsequently, this mixture was diluted 100-fold either with the respective

inhibitor at the original concentration or assay buffer. The substrate (Z-Lys(Ac)-AMC (ZMAL)) and trypsin were added to all samples and the time-dependent in situ AMC release was monitored continuously following our previously reported protocol.[57] In the case of the 100-fold jump dilution of vorinostat (Figure 5B, left), HDAC6 regained full deacetylase activity compared to blank (DMSO 1%) which is in excellent agreement with the fast-on/fast-off binding behavior of vorinostat. Conversely, the HDAC6 activity could not be restored after 100-fold dilution of **6** (Figure 5B, middle), hence indicating that **6** or the ring-opened acylhydrazide **13** disengages very slowly from HDAC6. Dialysis experiments with 10,000-fold excess of buffer over 21 hours confirmed the tight-binding properties of **6** (Figure 5C), suggesting that the unique binding mode of **6** leads to essentially irreversible inhibition of HDAC6. In contrast, the deacetylase activity of HDAC6 was nearly completely restored after the 100-fold jump dilution of **14** (Figure 5B, right). These results indicate that the closely related analogs **6** (tight-binding, essentially irreversible inhibitor) and **14** (fast-off binding properties) differ in their dissociation behavior and might therefore act *via* different modes of action.

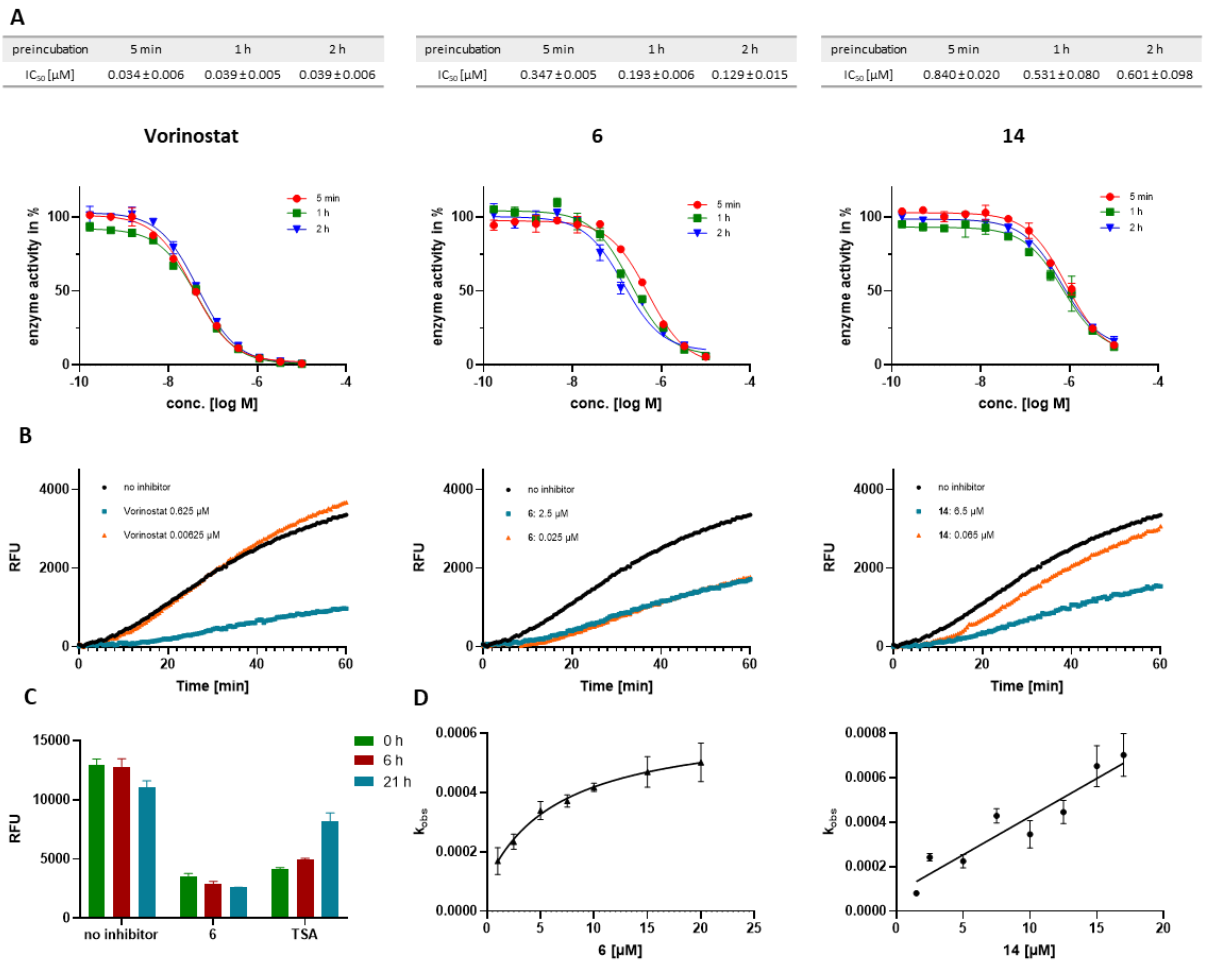

Figure 5. Analysis of the association and dissociation behavior of **6** and **14** at HDAC6. **A**: Representative dose-response curves and IC_{50} values of vorinostat (left, control), **6** (middle), and **14** (right) after preincubation with HDAC6 for 5, 60, and 120 min. **B**: Progression curves of 100-fold jump dilution experiments with vorinostat (left, control), **6** (middle), and **14** (right) at HDAC6. Inhibitor concentrations are indicated on the left. Fluorescence of cleaved AMC is measured in relative fluorescence units (RFU). **C**: Recovered HDAC6 activity from samples incubated with DMSO, **6**, and trichostatin A (TSA, control) after dialysis against 10.000-fold excess fresh buffer. **D**: The apparent first-order rate constant k_{obs} (mean ± SD) was plotted against the corresponding inhibitor concentrations [I]. The resulting curves were fitted into Equation 2 or 3 (see Supporting Information). (left) **6**: the hyperbolic relationship between k_{obs} and [I] indicates slow-binding, "induced-fit" mechanism II; (right) **14**: the linear relationship between k_{obs} and [I] indicates slow-binding mechanism I.

The trifluoro analogue **14** similarly undergoes HDAC6-catalyzed ring opening based on LC-MS analysis of the product mixture resulting from incubation with HDAC6 HDAC6 (Figure S3 and S4, Supporting Information). However, in contrast with DFMO analogue **13**, jump dilution experiments with **14** revealed that it binds to HDAC6 reversibly. The crystal structure of the HDAC6–**13** complex shows that the difluoro moiety binds in a small pocket defined in part by P571. We hypothesize that the trifluoro group of **14** is sufficiently larger than the difluoro group of **13** so as to destabilize binding of the trifluoro group in the P571 pocket, which results in reversible rather than irreversible inhibition. Substitution of the CHF_2 group of **13** with a CF_3 group to generate a model of **14** bound in the HDAC6 active site suggests a steric clash with the backbone carbonyl of G582 (Figure 6).

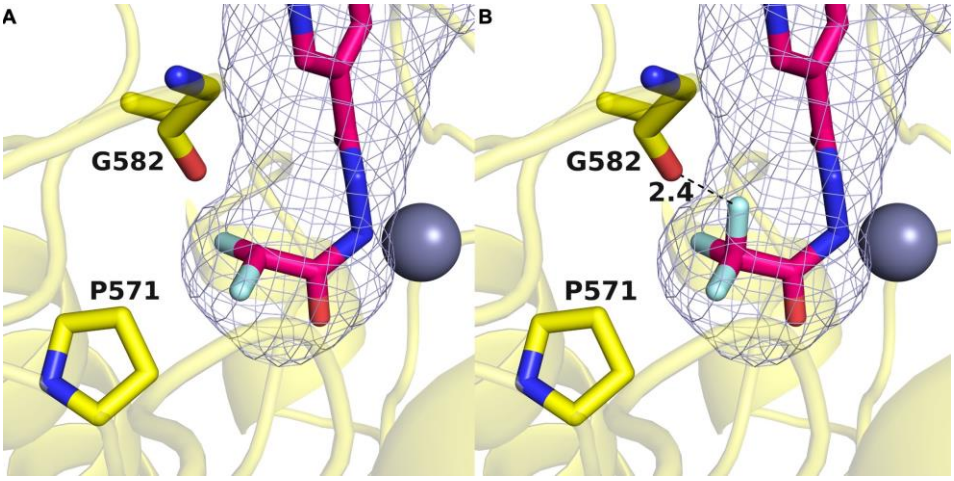

Figure 6. A: Binding pocket of HDAC6 in purple mesh generated by GetCleft showing the orientation of the difluoro group determined in the crystal structure of the complex with **13**. **B**: Substitution of the CHF_2 group with a CF_3 group yields a model of the complex with hydrolyzed **14** in the ring-opened form. The additional fluorine atom results in a clash with the backbone carbonyl of G582.

To confirm the hypothesis of different binding mechanisms for the difluoro and the trifluoro analogs, we performed HDAC6 kinetic studies. Our preincubation experiments demonstrated that **6** and **14** are slow-binding inhibitors of HDAC6. The most common types of slow-binding mechanisms are "simple slow-binding" (mechanism I) and "induced-fit" (mechanism II) (see Figure S1, Supporting information). While mechanism I represents a single-step slow-binding mode of inhibition, mechanism II is characterized as a two-step slow-binding inhibition mode. The slow-binding mechanisms I and II can be distinguished by their respective relationships between the rate constant for the onset of inhibition (k_{obs}) and the inhibitor concentration. To determine the binding mechanism of **6** and **14** at HDAC6, we utilized the *Progression-Method* and measured a series of progression curves using fixed concentrations of enzyme, substrate, and different inhibitor concentrations. Subsequently, the generated data were fitted into the Equation 1 (see Supporting Information) to calculate the k_{obs} values for the different inhibitor concentrations. The resulting k_{obs} vs inhibitor concentration plots are depicted in Figure 5D. In the case of **6** we observed a hyperbolic relationship between k_{obs} and the inhibitor concentration (Figure 5D, left), suggesting that **6** inhibits HDAC6 *via* the slow-binding "induced-fit" mechanism II. For **14** the relationship between inhibitor concentration and k_{obs} was linear (Figure 5D, right), indicating binding *via* the single-step slow-binding mechanism I. As discussed above, the DFMO **6** is hydrolyzed by HDAC6 and afterwards essentially trapped in the active site in a small pocket defined in part by P571, while the trifluoromethyl analog **14** is hydrolyzed and dissociates fast out of the enzyme. These differences might explain the different slow-binding mechanisms observed for **6** and **14**.

Proposed reaction mechanism

DFMO **6** is an essentially irreversible inhibitor of HDAC6, even though **13** does not form a covalent bond with any residues in the enzyme active site. We have determined that the

generation of acylhydrazide **13** requires the enzyme, i.e., **6** does not undergo slow hydrolysis over time to yield **13**. This implicates the reactive zinc-bound water molecule as the nucleophile for oxadiazole hydrolysis. Moreover, a mass shift of 2 is observed for acylhydrazide **13** when HDAC6 is incubated with **6** in $H_2{}^{18}O$ instead of $H_2{}^{16}O$. Subsequent hydrolysis of the ^{18}O-labeled acylhydrazide yields hydrazide **19** without the ^{18}O label (see Figure S5, Supporting Information). These results indicate that the ^{18}O label was contained in the second hydrolysis product, difluoroacetate, which further implies that the initial nucleophilic attack of zinc-bound water at oxadiazole **6** occurs exclusively at the C=N bond closest to the difluoro moiety. This indicates our proposed reaction mechanism depicted in Figure 7. The described C=N bond undergoes nucleophilic attack by the zinc-bound water molecule, leading to a tetrahedral intermediate. Electron rearrangement results in the ring opening of the oxadiazole, remaining in the deprotonated acylhydrazide. The negative charged nitrogen can strongly coordinate to the zinc ion, supporting the assumption for essential irreversible inhibition. Due to the crucial strong anionic zinc coordination, the proposed mechanism is in agreement with our results, that the synthetic acylhydrazide **13**, bearing a protonated nitrogen, does not show any inhibitory activity.

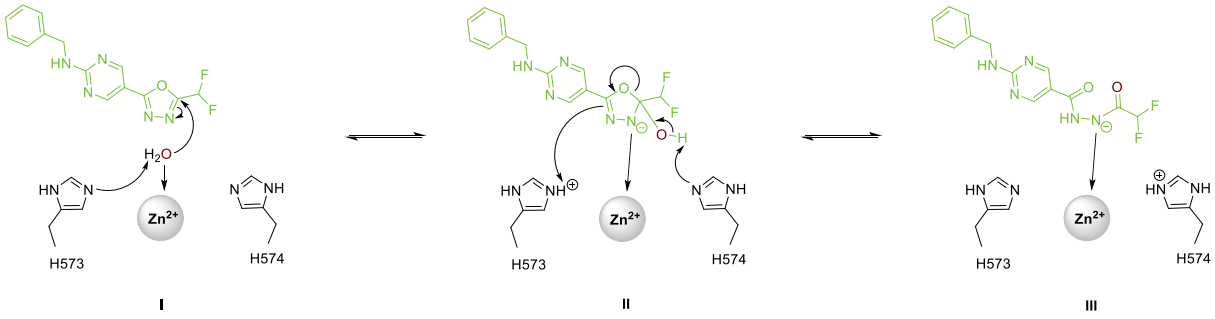

Figure 7. Proposed reaction mechanism of Zn^{2+} catalyzed ring opening reaction of DFMO compound **6**.

Conclusion

In summary, we have characterized the DFMO derivative **6** as potent and selective HDAC6 inhibitor. In IC_{50} shift experiments with various preincubation times compound **6** showed

slow-on binding properties with decreasing IC_{50} values. By analysis of the slow-binding characteristics we found that **6** inhibits HDAC6 *via* a two-step slow binding mechanism. To investigate the dissociation characteristics, we performed jump dilution experiments that revealed an essentially irreversible binding mode of DFMO **6** to its target. Additional dialysis experiments further confirmed the tight-binding properties of **6**. The trifluoromethyl analog **14**, on the other hand, acts as a slow-binding inhibitor following a single-step slow binding mechanism. In contrast to **6**, compound **14** was observed to disengage from the enzyme with fast-off binding properties in jump dilution assays, thus confirming that the two derivatives act *via* different modes of inhibition.

Using our crystallographic and mechanistic data, we are able to confirm that DFMOs serve as substrate analogs and therefore as mechanism-based inhibitors undergoing an HDAC6-catalyzed ring-opening reaction which is initiated by the attack of the zinc-bound water at the sp^2 carbon closest to the difluoromethyl moiety. Ultimately, this leads to the formation of the deprotonated acylhydrazide **13** as the active species. The analysis of the resulting HDAC6-**13** complex reveals an extensive array of intermolecular interactions that stabilize the bound inhibitor, particularly the strong anionic zinc coordination of **13** in combination with the binding of the difluoromethyl moiety in the P571 pocket. These structural features contribute to an exceptionally tight enzyme–inhibitor complex, thereby leading to an essentially irreversible inhibition of HDAC6.

Supplementary Information

Electronic Supplementary Information (ESI) available: Supplementary Figures, Schemes, Equations and Tables, experimental procedures, ^{1}H NMR, ^{13}C NMR and MS data.

Acknowledgements

B.K. acknowledges the Bonn International Graduate School of Drug Sciences (BIGS DrugS) for financial support of a research stay at the D.W.C. lab. We are grateful to Dr. Charles W. Ross III and Prof. Monica McCallum for their assistance with mass spectrometry experiments at the University of Pennsylvania. This research utilized the AMX beamline of the National Synchrotron Light Source II, a U.S. Department of Energy (DOE) Office of Science User Facility operated for the DOE Office of Science by Brookhaven National Laboratory under Contract

No. DE-SC0012704. The Center for BioMolecular Structure (CBMS) is primarily supported by the National Institutes of Health, National Institute of General Medical Sciences (NIGMS) through a Center Core P30 Grant (P30GM133893), and by the DOE Office of Biological and Environmental Research (KP1607011).

Conflicts of interest

There are no conflicts to declare.

Keywords: histone deacetylase • epigenetics • cancer • enzyme kinetics • HDAC6

References

[1] T. C. S. Ho, A. H. Y. Chan, A. Ganesan, *J. Med. Chem.* **2020**, *63*, 12460–12484.

[2] I. V Gregoretti, Y. M. Lee, H. V Goodson, *J. Mol. Biol.* **2004**, *338*, 17–31.

[3] J. Roche, P. Bertrand, *Eur. J. Med. Chem.* **2016**, *121*, 451–483.

[4] P. Wang, Z. Wang, J. Liu, *Mol. Cancer* **2020**, *19*, 1–21.

[5] M. Mielcarek, D. Zielonka, A. Carnemolla, J. T. Marcinkowski, F. Guidez, *Front. Cell. Neurosci.* **2015**, *9*, 1–9.

[6] M. Parra, E. Verdin, *Curr. Opin. Pharmacol.* **2010**, *10*, 454–460.

[7] C. Hubbert, A. Guardiola, R. Shao, Y. Kawaguchi, A. Ito, A. Nixon, M. Yoshida, X. F. Wang, T. P. Yao, *Nature* **2002**, *417*, 455–458.

[8] Y. Hai, S. A. Shinsky, N. J. Porter, D. W. Christianson, *Nat. Commun.* **2017**, *8*, 1–9.

[9] P. Bertrand, *Eur. J. Med. Chem.* **2010**, *45*, 2095–2116.

[10] J. H. Kalin, J. A. Bergman, *J. Med. Chem.* **2013**, *56*, 6297–6313.

[11] S. Shen, A. P. Kozikowski, *ChemMedChem* **2016**, *11*, 15–21.

[12] X. Zhang, Z. Yuan, Y. Zhang, S. Yong, A. Salas-burgos, J. Koomen, N. Olashaw, J. T. Parsons, X. Yang, S. R. Dent, T. Yao, W. S. Lane, E. Seto, *Mol. Cell.* **2007**, *27*, 197–213.

[13] T. J. Cohen, J. L. Guo, D. E. Hurtado, L. K. Kwong, I. P. Mills, J. Q. Trojanowski, V. M. Y. Lee, *Nat. Commun.* **2011**, *2*, 53.

[14] H. Ding, P. J. Dolan, G. V. W. Johnson, *J. Neurochem.* **2008**, *106*, 2119–2130.

[15] G. E. Karagöz, S. G. D. Rüdiger, *Trends Biochem. Sci.* **2015**, *40*, 117–125.

[16] C. Simões-Pires, V. Zwick, A. Nurisso, E. Schenker, P. A. Carrupt, M. Cuendet, *Mol. Neurodegener.* **2013**, *8*:7.

[17] J. P. Dompierre, J. D. Godin, B. C. Charrin, F. P. Cordelières, S. J. King, S. Humbert, F. Saudou, *J. Neurosci.* **2007**, *27*, 3571–3583.

[18] M. Brindisi, A. P. Saraswati, S. Brogi, S. Gemma, S. Butini, G. Campiani, *J. Med. Chem.* **2020**, *63*, 23–39.

[19] R. Adalbert, A. Kaieda, C. Antoniou, A. Loreto, X. Yang, J. Gilley, T. Hoshino, K. Uga, M. T. Makhija, M. P. Coleman, *ACS Chem. Neurosci.* **2020**, *11*, 258–267.

[20] M. Korfei, P. Mahavadi, A. Guenther, *Cells* **2022**, *11*, 1–45.

[21] G. Campiani, C. Cavella, J. D. Osko, M. Brindisi, N. Relitti, S. Brogi, A. P. Saraswati, S. Federico, G. Chemi, S. Maramai, G. Carullo, B. Jaeger, A. Carleo, R. Benedetti, F. Sarno, S. Lamponi, P. Rottoli, E. Bargagli, C. Bertucci, D. Tedesco, D. Herp, J. Senger, G. Ruberti, F. Saccoccia, S. Saponara, B. Gorelli, M. Valoti, B. Kennedy, H. Sundaramurthi, S. Butini, M. Jung, K. M. Roach, L. Altucci, P. Bradding, D. W. Christianson, S. Gemma, A. Prasse, *J. Med. Chem.* **2021**, *64*, 9960–9988.

[22] V. G. Magupalli, R. Negro, Y. Tian, A. V Hauenstein, G. Di Caprio, W. Skillern, Q. Deng, P. Orning, H. B. Alam, Z. Maliga, H. Sharif, J. J. Hu, C. L. Evavold, J. C. Kagan, F. I. Schmidt, K. A. Fitzgerald, T. Kirchhausen, Y. Li, H. Wu, *Science* **2020**, *369*:eaas8995.

[23] T. Hideshima, J. E. Bradner, J. Wong, D. Chauhan, P. Richardson, S. L. Schreiber, K. C. Anderson, *Proc. Natl. Acad. Sci. U. S. A.* **2005**, *102*, 8567–8572.

[24] T. Hideshima, P. G. Richardson, K. C. Anderson, *Mol. Cancer Ther.* **2011**, *10*, 2034–2042.

[25] S. Bhatia, V. Krieger, M. Groll, J. D. Osko, N. Reßing, H. Ahlert, A. Borkhardt, T. Kurz, D. W. Christianson, J. Hauer, F. K. Hansen, *J. Med. Chem.* **2018**, *61*, 10299–10309.

[26] D. T. Vogl, N. Raje, S. Jagannath, P. Richardson, P. Hari, R. Orlowski, J. G. Supko, D. Tamang, M. Yang, S. S. Jones, C. Wheeler, R. J. Markelewicz, S. Lonial, *Clin. Cancer Res.* **2017**, *23*, 3307–3315.

[27] S. J. Atkinson, P. E. Soden, D. C. Angell, C. Chung, K. A. Giblin, N. Smithers, R. C. Furze, L. Gordon, G. Drewes, I. Rioja, J. Witherington, N. J. Parr, R. K. Prinjha, *Med. Chem. Commun.* **2014**, *18*, 342–351.

[28] F. Tang, Z. Yang, Y. Tan, Y. Li, *npj Precis. Oncol.* **2020**, *4*, 1–7.

[29] W. Guerrant, V. Patil, J. C. Canzoneri, A. K. Oyelere, *J. Med. Chem.* **2012**, *55*, 1465–1477.

[30] H. Zhijun, W. Shusheng, M. Han, L. Jianping, Q. Li-sen, L. Dechun, *Tumor Biol.* **2016**, *37*,

10257–10267.

[31] J. H. Kalin, M. Wu, A. V Gomez, Y. Song, J. Das, D. Hayward, N. Adejola, M. Wu, I. Panova, H. J. Chung, E. Kim, H. J. Roberts, J. M. Roberts, P. Prusevich, J. R. Jeliazkov, S. S. Roy Burman, L. Fairall, C. Milano, A. Eroglu, C. M. Proby, A. T. Dinkova-Kostova, W. W. Hancock, J. J. Gray, J. E. Bradner, S. Valente, A. Mai, N. M. Anders, M. A. Rudek, Y. Hu, B. Ryu, J. W. R. Schwabe, A. Mattevi, R. M. Alani, P. A. Cole, *Nat. Commun.* **2018**, *8*:53.

[32] L. Morera, M. Lübbert, M. Jung, *Clin. Epigenetics* **2016**, *8*, 16.

[33] M. Wobser, A. Weber, A. Glunz, S. Tauch, K. Seitz, T. Butelmann, S. Hesbacher, M. Goebeler, R. Bartz, H. Kohlhof, D. Schrama, R. Houben, *J. Hematol. Oncol.* **2019**, *12*, 1–16.

[34] R. Ojha, H. L. Huang, W. C. HuangFu, Y. W. Wu, K. Nepali, M. J. Lai, C. J. Su, T. Y. Sung, Y. L. Chen, S. L. Pan, J. P. Liou, *Eur. J. Med. Chem.* **2018**, *150*, 667–677.

[35] S. Mehndiratta, M. H. Lin, Y. W. Wu, C. H. Chen, T. Y. Wu, K. H. Chuang, M. W. Chao, Y. Y. Chen, S. L. Pan, M. C. Chen, J. P. Liou, *Eur. J. Med. Chem.* **2020**, *185*, 111725.

[36] T. Liu, Y. Wan, Y. Xiao, C. Xia, G. Duan, *J. Med. Chem.* **2020**, *63*, 8977-9002.

[37] A. R. de Lera, A. Ganesan, *Curr. Opin. Chem. Biol.* **2020**, *57*, 135–154.

[38] S. He, G. Dong, Y. Li, S. Wu, W. Wang, C. Sheng, *Angew. Chem. Int. Ed.* **2020**, *59*, 3028–3032.

[39] I. N. Gaisina, W. Tueckmantel, A. Ugolkov, S. Shen, J. Hoffen, O. Dubrovskyi, A. Mazar, R. A. Schoon, D. Billadeau, A. P. Kozikowski, *ChemMedChem* **2016**, *11*, 81–92.

[40] Y. Depetter, S. Geurs, R. De Vreese, S. Goethals, E. Vandoorn, A. Laevens, J. Steenbrugge, E. Meyer, P. de Tullio, M. Bracke, M. D'hooghe, O. De Wever, *Int. J. Cancer* **2019**, *145*, 735–747.

[41] X.-H. Zhang, Qin-Ma, H.-P. Wu, M. Y. Khamis, Y.-H. Li, L.-Y. Ma, H.-M. Liu, *J. Med. Chem.* **2021**, *64*, 1362–1391.

[42] R. Jenke, N. Reßing, F. K. Hansen, A. Aigner, T. Büch, *Cancers* **2021**, *13*, 1–43.

[43] C. Y. Wang, L. H. Lee, *Antimicrob. Agents Chemother.* **1977**, *11*, 753–755.

[44] L. Zhang, J. Zhang, Q. Jiang, L. Zhang, W. Song, *J. Enzyme Inhib. Med. Chem.* **2018**, *33*, 714–721.

[45] K. Yue, S. Sun, G. Jia, M. Qin, X. Hou, C. J. Chou, C. Huang, X. Li, *J. Med. Chem.* **2022**, *65*, 12140–12162.

[46] Y. Kim, C. S. Lee, J. T. Oh, H. Song, J. Choi, J. Lee, **2017**, WO 2017/065473 A1

[47] I. Çakır, C. K. Hadley, P. L. Pan, R. A. Bagchi, M. Ghamari-Langroudi, D. T. Porter, Q. Wang, M. J. Litt, S. Jana, S. Hagen, P. Lee, A. White, J. D. Lin, T. A. McKinsey, R. D. Cone, *Nat. Metab*. **2022**, *4*, 44-59.

[48] T. Keuler, B. König, N. Bückreiß, F. B. Kraft, P. König, L. Schäker-Hübner, C. Steinebach, G. Bendas, M. Gütschow, F. K. Hansen, *Chem. Commun.* **2022**, *58*, 11087–11090.

[49] A. Cragin, P. R. Watson, B. König, F. K. Hansen, D. W. Christianson, *FASEB J.* **2022**, *36*, DOI https://doi.org/10.1096/fasebj.2022.36.S1.R3604.

[50] E. Cellupica, G. Caprini, P. Cordella, C. Cukier, G. Fossati, M. Marchini, I. Rocchio, G. Sandrone, M. A. Vanoni, B. Vergani, K. Źrubek, A. Stevenazzi, C. Steinkühler, *J. Biol. Chem.* **2023**, *299*, 102800.

[51] R. Huisgen, J. Sauer, H. J. Sturm, *Angew. Chemie* **1958**, *70*, 272–273.

[52] J. A. Bergman, K. Woan, P. Perez-Villarroel, A. Villagra, E. M. Sotomayor, A. P. Kozikowski, *J. Med. Chem.* **2012**, *55*, 9891–9899.

[53] V. Krieger, A. Hamacher, F. Cao, K. Stenzel, C. G. W. Gertzen, L. Schäker-Hübner, T. Kurz, H. Gohlke, F. J. Dekker, M. U. Kassack, F. K. Hansen, *J. Med. Chem.* **2019**, *62*, 11260–11279.

[54] D. Diedrich, A. Hamacher, C. G. W. Gertzen, L. A. Alves Avelar, G. J. Reiss, T. Kurz, H. Gohlke, M. U. Kassack, F. K. Hansen, *Chem. Commun.* **2016**, *52*, 3219–3222.

[55] W. Sippl, J. Melesina, C. V. Simoben, E. F. Bülbül, L. Praetorius, D. Robaa, *ChemMedChem* **2021**, *16*, 1336-1359.

[56] Y. Hai, D. W. Christianson, *Nat. Chem. Biol.* **2016**, *12*, 741–747.

[57] L. Schäker-Hübner, R. Haschemi, T. Büch, F. B. Kraft, B. Brumme, A. Schöler, R. Jenke, J. Meiler, A. Aigner, G. Bendas, F. K. Hansen, *ChemMedChem* **2022**, *17*, e202100755.

[58] Y. Jiang, J. Xu, K. Yue, C. Huang, M. Qin, D. Chi, Q. Yu, Y. Zhu, X. Hou, T. Xu, M. Li, C. J. Chou, X. Li, *J. Med. Chem.* **2022**, *65*, 285–302.

[59] K. Yue, S. Sun, G. Jia, M. Qin, X. Hou, C. J. Chou, C. Huang, X. Li, *J. Med. Chem.* **2022**, *65*, 12140–12162.